Adaptive V2G Peak Shaving and Smart Charging Control for Grid Integration of PEVs

Fatih Erden, Mithat C. Kisacikoglu, and Nuh Erdogan

***Abstract*—The stochastic nature of plug-in electric vehicle (PEV) driving behavior and distribution grid load profile make it challenging to control vehicle-grid integration in a mutually beneficial way. This study proposes a new adaptive control strategy that manages PEV charging/discharging for peak shaving and load leveling in a distribution grid. For accurate and high fidelity transportation mobility modeling, real vehicle driving test data are collected from the field. Considering the estimated total required PEV battery charging energy, the vehicle-to-grid capabilities of PEVs, and the forecasted non-PEV base load, a reference operating point for the grid is estimated. This reference operating point is updated once at the end of peak hours to guarantee a full final state-of-charge to each PEV. Proposed method provides cost-efficient operation for the utility grid, utmost user convenience free from range anxiety, and ease of implementation at the charging station nodes. It is tested on a real residential transformer, which serves approximately one thousand customers, under various PEV penetration levels and charging scenarios. Performance is assessed in terms of mean-square-error and peak shaving index. Results are compared with those of various reference operating point choices and shown to be superior.**

***Index Terms*—Grid integration, peak shaving, plug-in electric vehicles (PEVs), smart charging, vehicle-to-grid (V2G).**

I. Introduction

The global decrease for fossil fuels, and the demand for more cost-effective, environment-friendly vehicles have forced the automotive sector to improve plug-in electric vehicle (PEV) technologies. It is expected in the near future that the ratio of PEVs in the vehicle market will progressively increase worldwide, especially in developed countries [1]. With a growing PEV market, the penetration of PEVs into the utility grid has become a matter of concern. PEV-grid integration may result in adverse effects, such as increased power demand and losses, voltage unbalance/voltage deviations, and need for additional network investments [2]–[4]. On the other hand, since personal vehicles are used for mobility for about only 4% of their lifetime, PEVs can co-operate with the utility grid to provide ancillary services when needed [5].

The vehicle-to-grid (V2G) integration framework enables PEVs to be controlled by the utility grid or aggregators by means of communication between vehicles and the grid. Unidirectional V2G (V1G) is used for PEV charging load management and load leveling (valley filling), whereas bidirectional V2G is used for peak shaving, spinning reserve, reactive power compensation, and support for intermittent renewable energy [6]–[10]. For each service, optimization objectives, such as load profile optimization, loss/cost/emission minimization [11]–[13], and revenue maximization [5] have been proposed. Each objective function has certain constraints due to power system operation and PEV mobility requirements, such as power balance between the supply and load, grid voltage limits, PEV availability, battery state of charge (SOC), and PEV charger limitations. To realize V2G, electric vehicle grid integration (EVGI) framework should be a) cost-efficient for the utility grid, b) user-convenient, and c) practical in the field to be adopted in the near future.

Among different objective functions for bidirectional V2G, peak shaving and valley filling has been the focus of mainstream research [7], [14]–[20]. The main objective is to minimize the peak power demand, while decreasing the total load variance so that utilization of the grid investments and operational efficiency would increase. This is achieved by charging the PEVs whenever the total load is lower than a reference operating point for the grid and discharging the PEVs whenever the total load is greater than the reference operating point. This point can be set by the utility [21] or aggregator [22]. The selection of the reference operating point plays an important role in meeting service quality and customer convenience [23]. In [22], the reference operating point is determined so as to maximize an aggregator profit, while in [21], it is selected to optimize the load profile for the utility. However, these solutions are based on a well-known base load profile and do not consider PEV loads. Several other fixed operating points have been proposed, such as the mean of the entire daily base load (DM) [18]–[20], [24], [25] and median of daily base load between minimum and maximum points (MMMP) [26]. However, these settings will not always give the best solution in terms of grid power quality. This happens especially when the distribution transformer has a low load factor, and it cannot accommodate even moderate PEV penetration without any charging control [27]. In such cases, variance of the total load may increase [27]. Therefore, a dynamic reference point should be adopted, which can handle different PEV penetration rates, user mobility, and base load profiles. This study proposes a dynamic approach to overcome such problems seen in a residential distribution network with about 1000 customers.

In terms of real-time controlling of PEV-grid integration, centralized [11], [13], [15], [24] or distributed (decentralized)

This paper has been accepted for publication in Electric Power Components and Systems. F. Erden is with Department of Electrical and Computer Engineering, North Carolina State University, Raleigh, NC 27606 (e-mail: ferden@ncsu.edu).

M. C. Kisacikoglu is with Department of Electrical and Computer Engineering, University of Alabama, Tuscaloosa, AL 35487 (e-mail: mkisacik@ua.edu).

N. Erdogan is with Marine and Renewable Energy Centre, University College Cork, Cork, Ireland (e-mail: nuh.erdogan@ucc.ie).

[19], [20], [28]–[32] control frameworks have been proposed. In general, distributed methods are low in computational complexity and more user convenient but centralized methods achieve better utilization of PEVs for grid support due to being cognizant of the grid. However, they suffer from communication and computational overhead. With respect to the topic centralized control, optimization of PEV-grid integration in terms of different technical objectives has been extensively researched in the literature [33]–[38]. It was shown in [33] and [34] that charging strategies with a technical objective (e.g., minimizing peak loads) can achieve more PEV accommodation for the utility grid without needing infrastructure updates. In the studies that involve optimal grid integration of PEVs, the problem can either be formulated with deterministic models, such as convex or linear [35], [36], or as meta-heuristic optimization models such as an ant colony, particle swarm, and genetic algorithm [33], [37], [38]. The global optimal solution found in these studies requires that the load profile and PEV mobility parameters are perfectly known, which is not the case in reality, especially for small scale distribution networks. Furthermore, the meta-heuristic solutions can be very time inefficient. In [33], PEV charging rates are optimized only on a half-hourly basis to prevent violation of real-time computational restrictions. In [37], an ant colony optimization based approach requires around 127s to find the best route for a PEV which is prohibitive to be implemented in real-time. These issues indicate that seeking the optimal solution for PEV-grid integration makes it less practical for real-time field implementation. Therefore, controllers that are time-efficient and robust against grid dynamics and PEV mobility are needed for better performance in the field.

In addition, user convenience and ease of interaction also contribute to the practicability of a V2G algorithm. That is, they should have minimal computational complexity and include a heterogeneous EVGI framework; i.e., different vehicle models, charging station type/limits, and compliance with the standards. In [7], a PEV user has to provide complex information, such as level of peak shaving index (PSI) which cannot be requested from the users. In [39], an intermittent renewable energy source is tracked without guaranteeing a fully charged PEV at the time of departure which violates user satisfaction. While PEV mobility profile determines the amount of regulation up-and-down capacity, including service period, its stochastic nature is ignored in [21], [23], [33], [34]. Moreover, user convenience is often regarded as SOC at departure time in the morning [19], [23]. A minimum driving range for any emergency trips that might occur during charging/discharging should be considered for a realistic case study.

This study proposes a new adaptive control strategy to manage PEV charging/discharging operation within a neighborhood of approximately 1000 mostly-residential customers supplied by a distribution transformer with a low load factor. The main goal is to flatten the residential distribution transformer load profile on a 24-hour basis without compromising PEV user convenience (full SOC at time of departure). For this purpose, a mobility model is built first from real driving data collected from the field. Based on this model, charge energy needs and V2G capabilities of PEVs are estimated, and a reference operating point (P_{ref}) for the transformer is determined. Then, a real-time algorithm computes the difference between the total load and P_{ref} as a function of time. Each PEV participating into V2G service is discharged in varying power rates such that the discharging profiles track this difference curve. After computing actual charge needs of all PEVs at the end of the peak-period, the reference operating point and, hence, the difference curve is updated to ensure a full charge for all PEVs at departure time. Finally, the charging profile for each PEV is adjusted accordingly and night-valley is filled. This computation is accomplished without needing to run a computationally intense optimization algorithm. Test scenarios are developed using up-to-date EVGI experimental field data, a real non-PEV base load, and PEV mobility data. Results are compared with those of other state-of-the-art techniques in terms of PSI and mean-square-error (MSE).

In this respect, the main salient contributions of this study can be summarized as follows:

- A new reference operating point calculation method for the grid is proposed based on the non-PEV base load forecast and available PEV mobility statistics. Since this approach also makes use of the mobility statistics, it achieves a lower aggregated load variance in comparison to the approaches assuming a fixed reference operating point.
- A new adaptive controller is developed so that discharging profiles of PEVs participating in the V2G process are only updated at the time when a new PEV is connected to the grid. This makes the proposed approach adaptive to deviations from the assumed mobility model and provides a closer fit to the reference operating point. It also eliminates the need to execute intensive real-time optimization calculations, which will be costly to implement at each central server location.
- Finally, this study shows that if the transformer base loading without PEVs can be predicted with a high accuracy, the algorithm can effectively reduce the total power consumption variance. It is not required to know the real-time overall power consumption of the region which will effectively reduce the need to install power meters at the substations.

The rest of the paper is organized as follows. Section II introduces the modeling of the EVGI framework and transportation mobility modeling. Section III describes the development of adaptive smart charging/discharging strategy. Case studies are presented in Section IV. Finally, conclusions are given in Section V.

II. System Description of the EVGI Framework

A. PEV-Grid Integration System Architecture

Five different PEVs, listed in Table I, are used. Each of the chargers used in this work is assumed to have a constant 90% operating efficiency and 1.0 power factor at all operating points [27]. None of the production vehicles listed in Table I allow on-board V2G power transfer. However, off-board V2G can bypass the on-board charger and reach the battery ports

TABLE I
TYPES OF PEVS AND THEIR SPECIFICATIONS.

Vehicle Make and Model	Vehicle Type	Usable Batt. Size (kWh)	EV Range (mi)	Max. Onboard Charging Power (kW)
BMW i3	EV	18.8	81	7.4
Chevrolet Volt	PHEV	14	53	3.3
Nissan Leaf	EV	30	107	6.6
Chevrolet Bolt	EV	60	238	7.2
Tesla Model S	EV	70	240	10

using the Chademo/Combo connector. Utility service providers may install off-board V2G units at the required locations in the distribution system to utilize available PEV energy storage upon agreement with vehicle users/manufacturers. Therefore, for a more realistic scenario, this study assumes that vehicles provide V2G service with off-board charging units, rated at 30 kW and use their on-board chargers for unidirectional charging.

Fig. 1 summarizes the described system architecture. Each electric vehicle supply equipment (EVSE) or V2G charging station communicates with the control center using a wireless/wired communication set-up. Vehicle-station communication is employed through the low-level and high-level communication over the control pilot. Related high-level vehicle information can be transferred between the EVSE/off-board station and the PEV through power line communication over the control pilot pin utilizing standards such as ISO 15118 [40].

B. Modeling of the User Preferences

As the vehicles and their grid integration are modeled, user preferences should also be considered to evaluate the performance of the algorithm. There are three types of user charging profiles modeled in this study:

i) Uncontrolled charging: PEV charges at rated on-board charging power when connected to the grid. No control over charging is allowed. Charging ends when the vehicle is fully charged.

ii) Smart charging: PEV starts charging with a smart charging profile after peak hours. If the PEV has a lower driving range than a minimum required at arrival, it starts charging immediately until minimum EV range is regained. The minimum range is defined as an average distance to important destinations, i.e., hospitals, drug stores, shops, and so forth. This distance is assumed to be 50 km within the city of Ankara. Then, the PEV implements the smart charging algorithm described in Section III. Charging ends at the morning departure time with fully charged battery.

iii) V2G service: This is the most sophisticated and grid-friendly charging profile. It charges/discharges PEVs during the entire grid-connected parking period. The minimum driving range is again retained for emergency trips. Charging ends at the morning departure time with fully charged battery.

V2G operation can take place using only off-board charging stations installed by the utility company. To sign-up for the V2G service, PEVs must have a higher SOC than the charge level required for emergencies. This is to make sure that off-board stations are not used to increase the peak demand, but, rather, are utilized to help with peak shaving. A first-come, first-served basis is used. Users who are eligible to connect their vehicles to off-board charging units are automatically enrolled in the V2G service. Users who enroll in this service will have an increased aging rate for their batteries due to increased partial cycles depending on the battery capacity, battery operation temperature, and drive cycle [41]. The additional cost due to battery wear should be covered by the utility service provider asking this service from the PEVs. However, the battery wear analysis involves a detailed in-depth impact study, which is not in the scope of this paper. It is important to note that depth of discharge (DoD) is also an important factor affecting the battery lifetime. In this paper, we have preserved a limited DoD during V2G service by introducing an emergency range for each PEV. This helps to increase battery lifetime as opposed to discharging PEVs to their allowable minimum SOC.

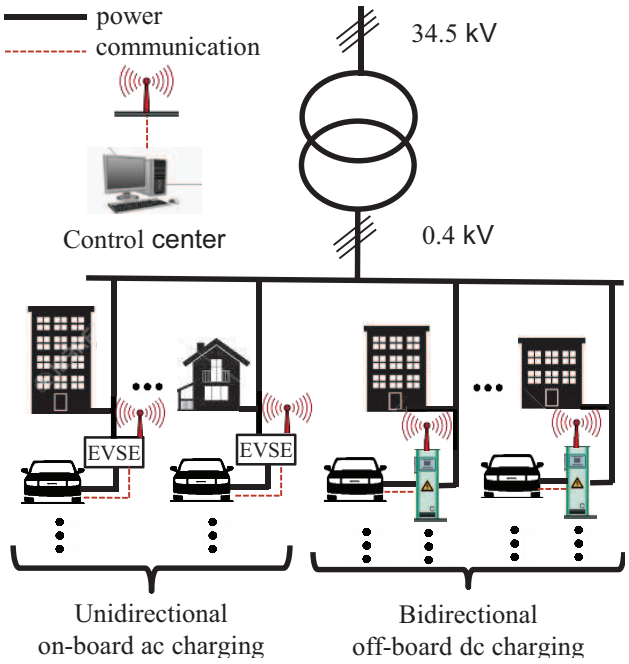

Fig. 1. EVGI architecture in the distribution system.

C. Transportation Mobility Modeling

The daily home arrival/departure times and trip distance data of 10 personal vehicles over a time period of one year was collected by EnerjiSA Baskent Electric Distribution Company [42] within the context of this study to form a realistic mobility model [43]. These data are collected using GPS tracking devices at each vehicle. Daily trip distances between 10 km-80 km, home arrival times after 4:00pm, and departures between 5:00am-10:00am are considered. Histograms of the collected data are shown in Fig. 2. It is observed that all three histograms resemble normal distributions so that a Gaussian curve can be fitted to each. The distribution fits are found to be $\mathcal{N}$(7h47, 0h23), $\mathcal{N}$(19h55, 1h40), and $\mathcal{N}$(39.5 km, 15.8 km) for home departure time, arrival time, and daily trip distance data, respectively, where $\mathcal{N}(\mu, \sigma)$ denotes a normal distribution with mean μ and standard deviation σ. It is also verified that the histograms mostly satisfy the well-known 68-95-99.7 statistics for fitted distributions. Therefore, PEV

mobility data are populated based on the aforementioned Gaussian characteristics. Finally, the PEVs are assumed to stay parked at home until the next departure time and occasional evening trips are ignored.

III. Development of Adaptive Smart Charging and Discharging Strategy

The proposed control algorithm considers the three user choices explained in Section II. Uncontrolled charging does not require any remote control, and hence is not considered here. Every PEV connected to the grid sends the following information to the control center once after plugging-in: user charging type, expected departure time in the morning, SOC at the time of grid connection (%), and PEV model-specific info, namely, on-board/off-board charger power (kW), average vehicle energy consumption rate (kWh/100km), and nominal battery capacity (kWh). The SOC and charging/discharging power reference are exchanged between EVSE and the control center every time when a PEV connects to or disconnects from the grid. Other inputs to the algorithm are the non-PEV base load forecast and the predetermined reference operating point for the grid.

Prior to proceeding with the details of the adaptive strategy, it is important to note the distinction between the offline and real-time stages of the algorithm. All of the upcoming load predictions (non-PEV base load and PEV loads based on the number of PEVs and their mobility characteristics) in the following subsection are made to estimate P_{ref} before the first PEV is connected to the grid. That is, P_{ref} is determined offline while all the remaining operations are carried out in real time. Section III-A describes the method to determine the reference operating points of the transformer during V1G and V2G services, while Section III-B and III-C explain the real-time computations of the algorithm.

A. Determination of Reference Operating Point

The fixed reference operating point approaches have difficulties in yielding a smooth load profile for different PEV penetration rates, user profiles, and transformer loading cases. However, it is possible to estimate a dynamic reference point that can deal with these uncertainties by using the historical data of PEV mobility and non-PEV base load.

In this study, the PEV penetration level and non-PEV load profile are assumed to be well estimated. For the calculation of the reference operating value, the enrollment to each plan option described in Section II-B are also assumed to be known a day in advance. The enrollments can either be done by user interface at the charging station or can be a contract-based subscription plan [44]. The enrollment data can be collected in the cloud and then used for day-ahead forecasting of user choices.

An iterative process is employed using the aforementioned assumptions. First, the reference operating point is initialized to the peak of day-time loading. Then, the net load including the uncontrolled PEV charging loads is estimated as:

$$\hat{p}_{net}(t)=\hat{p}_{load}(t)+\hat{p}_{uncon,only}(t)+\hat{p}_{uncon,emerg}(t), \quad (1)$$

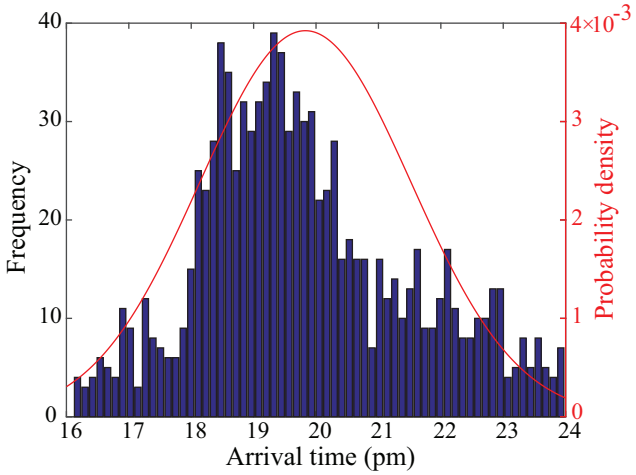

(a)

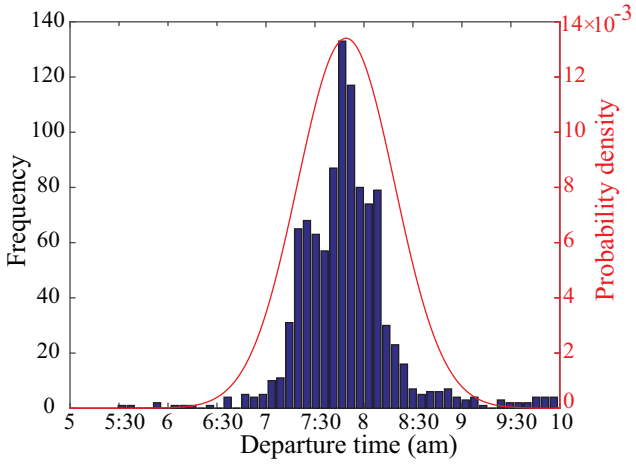

(b)

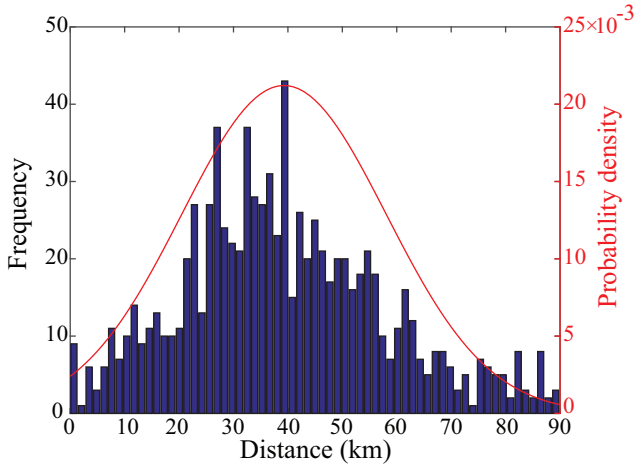

(c)

Fig. 2. Histogram of the collected data (bar) and corresponding Gaussian distribution fit (line) for (a) arrival time, (b) departure time, and (c) daily trip distances.

where $p_{load}(t)$ is the non-PEV base load, $p_{uncon,only}(t)$ is the total uncontrolled charging power of PEVs, while $p_{uncon,emerg}(t)$ is the total uncontrolled charging power of PEVs that are charged until minimum required range is regained, all in units of kW, and the hat symbol indicates the

estimate of the corresponding variable. Next, the estimated total peak energy $\hat{E}_{peak,total}$ is calculated using

$$\hat{E}_{peak,total} = \int_{t_{peak-start}}^{t_{peak-end}} (\hat{p}_{net}(\tau) - P_{ref}) \cdot d\tau, \quad (2)$$

where $t_{peak-start}$ and $t_{peak-end}$ are the times for the first and second intersections of $\hat{p}_{net}(t)$ and current reference point. The total V2G energy to be provided to the grid $\sum \hat{E}_{V2G}$ should be equal to $\hat{E}_{peak,total}$ at most, to prevent an undesirable valley in the evening. $\sum \hat{E}_{V2G}$ is taken to be equal to $\hat{E}_{peak,total}$, which is a reasonable approximation for even very low penetration rates. Then, the total charging energy can be found as:

$$\sum \hat{E}_{ch} = \sum \hat{E}_{trip} + \sum \hat{E}_{V2G} - \sum \hat{E}_{uncon-only} - \sum \hat{E}_{uncon-emerg}, \quad (3)$$

where $\sum \hat{E}_{trip}$ is the total estimated trip energy consumption, and $\sum \hat{E}_{uncon-only}$ and $\sum \hat{E}_{uncon-emerg}$ are the estimated energy needs, all in units of kWh, calculated using $\hat{p}_{uncon-only}(t)$ and $\hat{p}_{uncon-emerg}(t)$, respectively. Finally, the total energy of the night-valley is estimated using

$$\hat{E}_{valley,total} = \int_{t_{valley-start}}^{t_{dept,ave}} (P_{ref} - \hat{p}_{net}(\tau)) \cdot d\tau, \quad (4)$$

where $t_{valley-start} = t_{peak-end}$, and $t_{dept,ave}$ is the average departure time. Note that the upper bound of the integral in (4) might be selected differently, but it is observed that $t_{dept,ave}$ produces the best MSE performance. If $\sum \hat{E}_{ch} > \hat{E}_{valley,total}$, V2G support should be decreased, and hence P_{ref} increased. Otherwise, P_{ref} is decreased. The same process is repeated with the updated values in the following iterations until P_{ref} converges. The final value of the P_{ref} is assigned as the reference operating point.

The real-time algorithm described in Section III-B uses P_{ref} as a reference and adjusts discharging profiles of PEVs participating into V2G service. Since P_{ref} is determined based on the estimated parameters, charging PEVs with reference to P_{ref} cannot guarantee full charge of the PEVs. Therefore, the actual required total charge is calculated at the end of the peak-period, and P_{ref} is updated to satisfy $\sum E_{ch} = E_{valley,total}$. That means the actual total energy in the valley period is exactly equal to the actual total charge requirement. The reference value satisfying this equality is called the $P_{ref,night}$. The smart charging algorithm described in Section III-C uses $P_{ref,night}$ as the reference operating point and manages the charging process of PEVs.

B. V2G Discharging Algorithm

Let j denote the number of uncontrolled charging PEVs, k denote the number of smart charging PEVs, m (where $m \leq k$) be the number of PEVs with smart charging but have less than 50 km range, and n be the number of PEVs participating into V2G service. The total number of PEVs at a time t is equal to $j + k + n$. All these variables are functions of time and updated in real-time as new PEVs are plugged in. Note that the number of PEVs of different choices are not assumed to be known ahead of time making the strategy adaptive to varying conditions. The peak power to be shaved using V2G algorithm is calculated as:

$$p_{peak}(t) = \hat{p}_{load}(t) + p_{uncon-total}(t) - P_{ref}, \quad t_{peak-start} < t < t_{peak-end}, \quad (5)$$

where $p_{uncon-total}(t)$ is the sum of uncontrolled charging power of PEVs and PEVs with less than 50 km range at the time of grid connection. Therefore,

$$p_{uncon-total}(t) = \sum_{i=1}^{j(t)} p_{uncon-only,i}(t) + \sum_{i=1}^{m(t)} p_{uncon-emerg,i}(t). \quad (6)$$

Furthermore,

$$p_{uncon-only,i}(t) = \begin{cases} P_i^{rated} & \text{for } SOC_i(t) < 100\% \\ 0 & \text{for } SOC_i(t) = 100\% \end{cases} \quad (7)$$

$$p_{uncon-emerg,i}(t) = \begin{cases} P_i^{rated} & , SOC_i(t) < SOC_{emerg,i}(t) \\ 0 & , SOC_i(t) \geq SOC_{emerg,i}(t) \end{cases} \quad (8)$$

$$SOC_i(t) = SOC_i(t_{0,i}) + \frac{P_i^{rated} \cdot (t - t_{0,i})}{C_{B,i}} \cdot \eta, \ t > t_{0,i}, \quad (9)$$

where $SOC_{emerg,i}$ is the SOC level needed for 50 km range (%), P_i^{rated} is the rated on-board charging power (kW), $t_{0,i}$ is the arrival time (h), and $C_{B,i}$ is the battery capacity (kWh) for the i^{th} PEV. $p_{uncon-only,i}(t)$ is the uncontrolled charging power for the i^{th} PEV, while $p_{uncon-emerg,i}(t)$ is the uncontrolled charging power until the i^{th} PEV reaches its emergency SOC. Using (5), the total energy to be shaved from time t till the end of the peak period can be calculated as:

$$E_{peak}(t) = \int_{t}^{t_{peak-end}} p_{peak}(\tau) \cdot d\tau, \quad t_{peak-start} < t < t_{peak-end}. \quad (10)$$

Then, the total available PEV V2G energy at a time during peak hours has to be found as:

$$E_{av-total}(t) = \sum_{i=1}^{n(t)} E_{av,i}(t), \ t_{peak-start} < t < t_{peak-end}. \quad (11)$$

where, $E_{av,i}(t)$ is the available energy of i^{th} PEV at time t. The available energy corresponds to a charge of $(SOC_i(t) - SOC_{emerg,i})$. Each PEV signing into V2G service acknowledges sending a total energy to the grid that is proportional to its available energy stored in its battery. If the total available energy is less than the energy desired to be shaved, the total available energy is utilized. Otherwise, to prevent creation of a valley during the peak shaving process, the definition of available energy is updated for each vehicle such that the total available energy is equal to the energy to be shaved, i.e.,

$$E_{av,i}(t) = \begin{cases} \frac{E_{av,i}(t)}{E_{av-total}(t)} \cdot E_{peak}(t) \ , & E_{av-total}(t) > E_{peak}(t) \\ E_{av,i}(t), & E_{av-total}(t) \leq E_{peak}(t) \end{cases} \quad (12)$$

As more vehicles join the V2G service, each vehicle's share for V2G support may decrease depending on (12). In addition, when the total available energy becomes equal to the required

peak shaving energy $E_{peak}(t)$, the total energy support is kept equal to $E_{peak}(t)$. Each PEV has to discharge a certain way at every time step to meet its discharged energy goals. Since the demand load is dynamic in nature, this study proposes an *adaptive* V2G control algorithm for each PEV tracing the load demand profile. To do so, the demand load curve to be shaved $p_{peak}(t)$ is divided into one-minute intervals. The total required V2G energy for a single interval can be calculated as follows:

$$\Delta E_{peak}(t) = \int_{t}^{t+1} p_{peak}(\tau) \cdot d\tau. \tag{13}$$

If one vehicle sends a total energy of $E_{av,i}(t)$ to shave a total peak energy of $E_{peak}(t)$ during the entire peak period, then similarly, to shave a total energy of $\Delta E(t)$ at one step, each vehicle has to send an energy for one time step as:

$$\Delta E_{V2G,i}(t) = \frac{\Delta E_{peak}(t)}{E_{peak}(t)} \cdot E_{av,i}(t). \tag{14}$$

Finally, the discharging power for the i^{th} PEV at any time during the peak hours is:

$$p_{V2G,i}(t) = \frac{\Delta E_{V2G,i}(t)}{\Delta t}. \tag{15}$$

The overall procedure, described by (5)-(15), is summarized in Fig. 3. $p_{V2G,i}(t)$ is simultaneously sent to every vehicle that signed into V2G service. In (15), $p_{V2G,i}(t)$ is checked to ensure its value is at most 30 kW, which is the rated power of the off-board charging station. If $\frac{\Delta E_{V2G,i}(t)}{\Delta t} \geq 30kW$, then $p_{V2G,i}(t)$=30 kW is taken.

C. V1G Smart Charging Algorithm

PEVs, except the ones continuing to uncontrolled charging, start smart charging at the end of the peak-period. That is, the number of PEVs doing smart charging during the night is $n + k$. It is important to remind that m of $n + k$ PEVs start smart charging after they reach the minimum emergency range. The aim of smart charging is to $dynamically$ fill the night-valley with $n + k$ PEVs and obtain a flat loading profile throughout the night.

The algorithm starts by defining the required valley filling power $p_{valley}(t)$. It is defined similar to $p_{peak}(t)$ as:

$$p_{valley}(t) = P_{ref,night} - \hat{p}_{load}(t) - p_{uncon-total}(t), \quad t_{valley-start} < t < t_{valley-end}. \tag{16}$$

with the difference that a new point-of-load value $P_{ref,night}$ is substituted for P_{ref}. This is to ensure that each PEV is fully charged by the departure time. $P_{ref,night}$ is calculated using the approach explained in Section III-A with actual charge requirements, which are no longer uncertain. Since the valley begins when peak ends, $t_{valley-start}$ in (16) is equal to $t_{peak-end}$. The theoretical value for the end time of the valley is the second intersection between $P_{ref,night}$ and grid load profile. However, as the time of operation is constrained by the PEV that leaves the latest, $t_{valley-end}$ is selected to be equal to the latest departure time, $t_{dept-max}$. Therefore, the required energy to fill the valley is calculated as:

$$E_{valley,i}(t) = \int_{t}^{t_{dept,i}} p_{valley}(\tau) \cdot d\tau, \; t_{valley-start} < t < t_{dept,i} \tag{17}$$

where, $t_{dept,i}$ is the departure time of the i^{th} PEV. (17) indicates that the definition of $E_{valley}(t)$ is different for each PEV and depends on its departure time. The required energy at time t to fully charge the i^{th} PEV can be calculated as:

$$E_{ch,i}(t) = (1 - SOC_i(t)) \cdot \frac{C_{B,i}}{\eta}. \tag{18}$$

Having determined the energy requirement to fill the valley and fully charge the PEVs, the charging profile of each PEV at every time step is calculated. A similar approach to that of the previous subsection is followed. First, $p_{valley}(t)$ is divided into one-minute intervals. Then, the total valley energy for each sampling time is

$$\Delta E_{valley,i}(t) = \int_{t}^{t+1} p_{valley}(\tau) \cdot d\tau, \; t_{valley-start} < t < t_{dept,i}. \tag{19}$$

Using (18) and (19), the required energy for charging i^{th} PEV can be calculated as:

$$\Delta E_{ch,i}(t) = \frac{\Delta E_{valley,i}(t)}{E_{valley,i}(t)} \cdot E_{ch,i}(t). \tag{20}$$

Finally, the smart charging power at time t for each PEV is:

$$p_{ch,i}(t) = \frac{\Delta E_{ch,i}(t)}{\Delta t}. \tag{21}$$

In (21), $p_{ch,i}(t)$ is checked to ensure that it does not exceed its rated power. If $\frac{\Delta E_{ch,i}(t)}{\Delta t} \geq P_i^{rated}$, then $p_{ch,i}(t) = P_i^{rated}$ is taken. The flow chart summarizing (16)−(21) is shown in Fig. 4.

IV. Case Studies

A. Analysis of Distribution Transformer Loading

The distribution network of Ankara, a city in Turkey, which is operated by Baskent Electricity Distribution Company is selected to test the proposed control algorithm. The non-PEV base load data were recorded for four months using a power quality meter. The meter was installed at a secondary site with a 34.5 kV/0.4 kV, 1000 kVA distribution transformer serving 985 residential customers. The measurements were recorded with a sampling time of ten minutes. The daily average active power load profile for weekdays over a period of four months (Sep–Dec 2014) is shown in Fig. 5. Among the available months, November is chosen as the base load profile for the test cases. An average peak/lowest demand of 240 kW/100 kW occurs around 8pm/5am during a weekday in November with a daily mean of 143 kW. The triple tariff periods (1, 2, and 3) correspond to night (10pm-6am), day-time (6am-5pm) and peak-time (5pm-10pm) hours, respectively. Peak loading mostly occurs in period 3 but extends into period 1 as well. Most part of the load profile in period 2 cannot be modified due to the unavailability of PEVs.

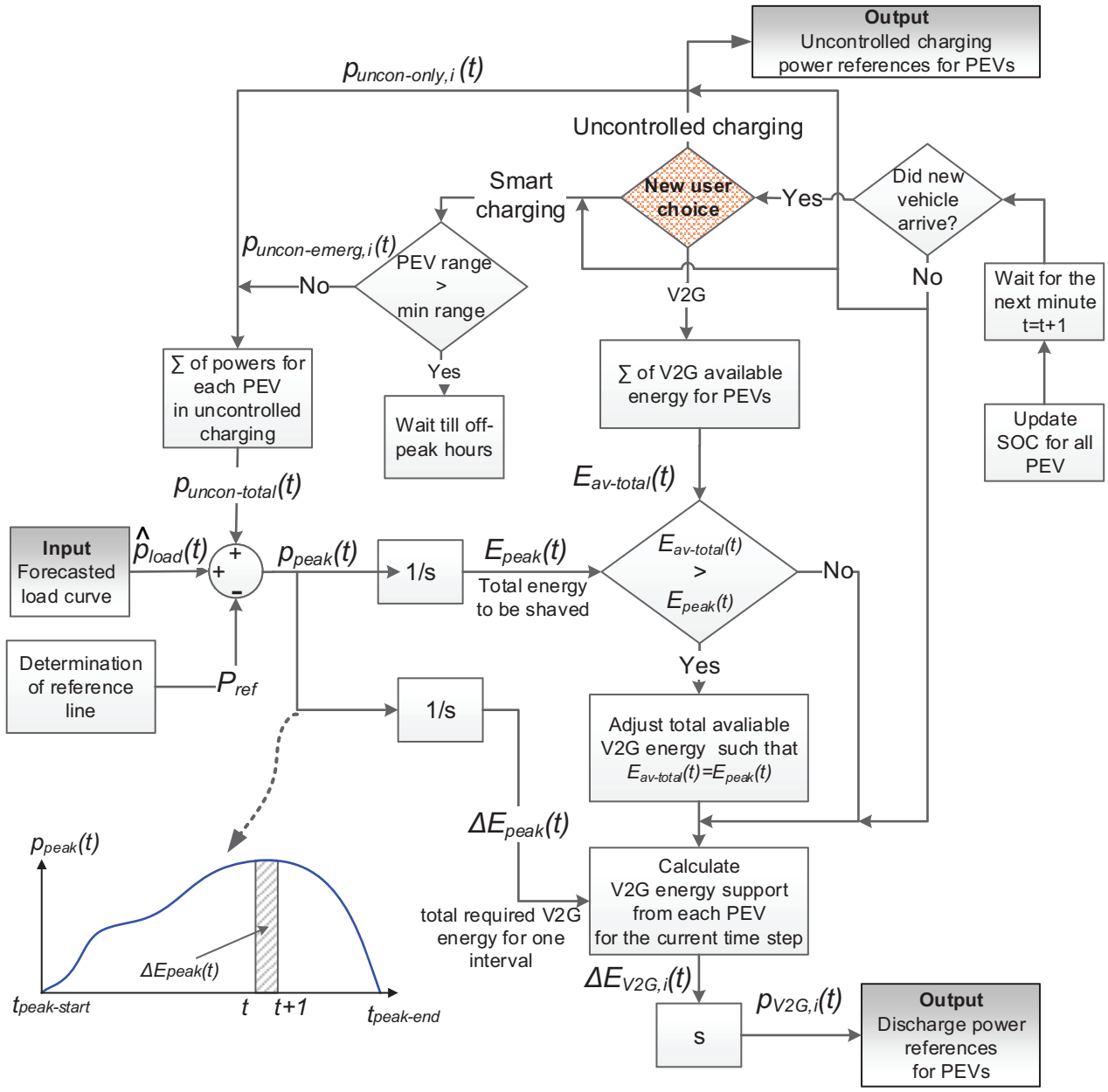

Fig. 3. Proposed V2G adaptive control algorithm flowchart.

B. Numerical Simulations

The impact of the proposed algorithm is quantified in this section. The vehicle models described in Table I are distributed homogeneously among all PEV users, and the corresponding trip parameters are determined as described in Section II-C. Each PEV user selects one of the three profiles at the time of plugging-in: (i) uncontrolled charging, (ii) smart charging, or (iii) V2G service. The participation ratio is assumed to be 20% for uncontrolled charging, 40% for smart charging, and 40% for V2G service among all users. Three different PEV penetration rates are assumed as roughly 5%, 10%, and 20% to account for different market adoption rates, and each household is assumed to possess one vehicle. These ratios correspond to about 50, 100 and 200 vehicles for 985 customers in the neighborhood. Moreover, the impact of reference operating point choice is analyzed for four different reference point selections, i.e., DM, MMMP, mean of peak hours (MPH) and proposed dynamic reference point. Therefore, a total of 12 different cases are studied.

The proof of concept is demonstrated for 10% PEV penetration level. The simulation is run 100 times, spanning a wide range of scenarios, for which performance of the proposed algorithm is assessed. Positive power represents charging/load consumption whereas negative power represents discharge in all figures. Fig. 6 shows aggregated load profile $(p_{load}(t)+p_{uncon-total}(t))$ with 10% PEVs for each simulated case. The resulting load after implementing the proposed algorithm is depicted in Fig. 7. As illustrated, PEVs are able to shave the most of the peak and fill the valley between

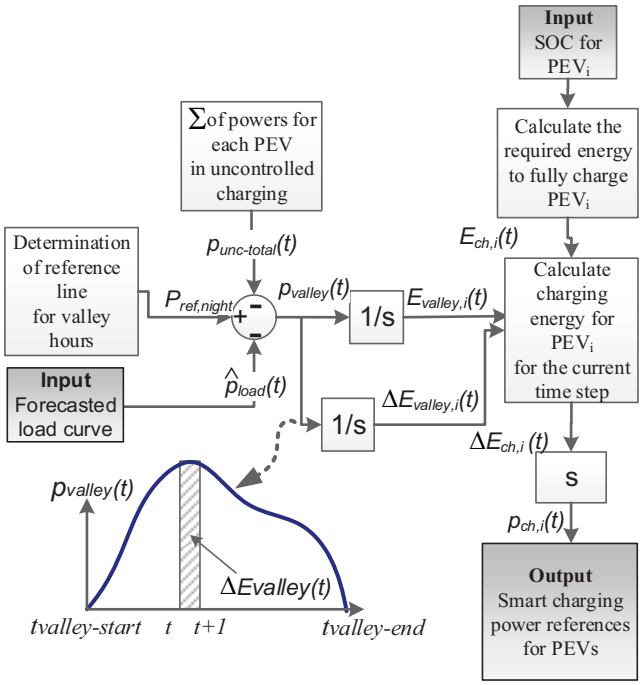

Fig. 4. Proposed smart charging algorithm flowchart.

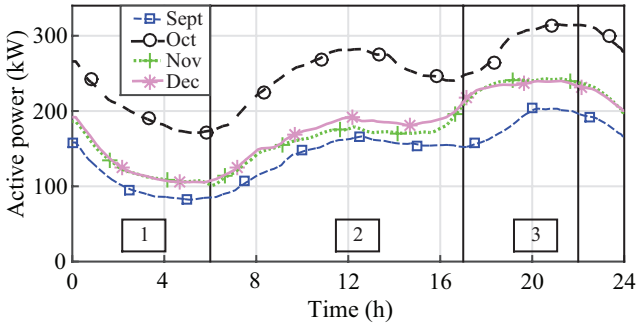

Fig. 5. Daily average active power demands for four months (non-PEV).

$t_{peak-start}$ (17:24) – $t_{dept-ave}$ (07:47), but are not available for grid services in the remainder of the day due to mobility.

To have a closer look at the individual power profiles of each different user profile group, the results of a single-run for a weekday are demonstrated in Fig. 8. Fig. 8(a) shows that the users who chose the uncontrolled charging option initiate their charging at the rated on-board charging power when they plug-in. The charging is not interrupted nor discretized until full SOC. Fig. 8(b) shows the power consumption of the users who select smart charging. It demonstrates the emergency charging power required during evening hours for the vehicles arriving with less than 50 km driving range. Their remaining charge is postponed until after $t_{peak-end}$ or when they are finished with emergency charging, whichever comes the latest. For this individual single-run, $t_{peak-end}$ is calculated to be 23:40. After $t_{peak-end}$, PEVs start smart charging to top off the valley to reach $P_{ref,night}$.

Fig. 8(c) shows the profile for PEVs joining the V2G service. During the evening hours, PEVs shave the peak and send power to the grid until $t_{peak-end}$. They act as a peaking power source for the utility grid and reduce the demand for

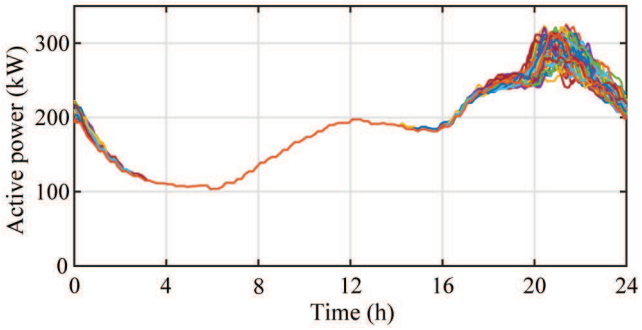

Fig. 6. Aggregated load profile with uncontrolled charging for 10% PEV penetration for 100 simulation runs.

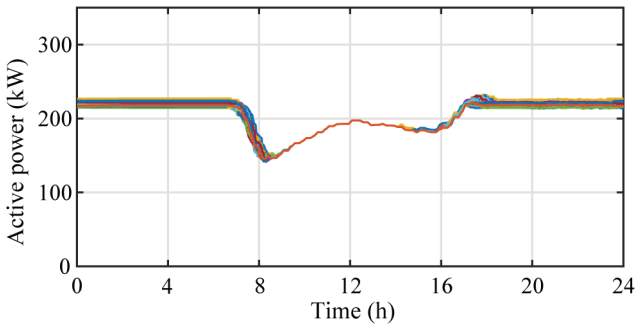

Fig. 7. Aggregated load profile with proposed algorithm for 10% PEV penetration for 100 simulation runs.

extra generation for the neighborhood. After $t_{peak-end}$, they join smart charging PEVs to help balance the valley. Fig. 8(d) shows the SOC values for individual vehicles and demonstrates that each and every PEV reaches a full SOC in the morning to provide the most user convenience, irregardless of the the charging option chosen.

Fig. 9(a)–(c) summarize the result of the proposed algorithm for the cases of 5%, 10%, and 20% penetration over an average of 100 random mobility trials. At 5% and 10%, the resulting load profile becomes level after the arrival of the required number of PEVs satisfying the V2G service criteria. Compared to the 5% case, the time at which the load profile flattens is earlier than that of the 10% case. The load profile is levelled for the entire peak-period of the 20% case since the number of PEVs participating into V2G service is enough to shave the peak.

The position of the reference line differs for each penetration level, which shows the benefits of the proposed method. It is the highest for the 20% case since the total expected trip energy consumption $\sum \hat{E}_{trip}$ is the largest for that case. In addition, the reference operating point is forecasted based on the assumption that the peak can be fully shaved, which is not the case for the 5% and 10% cases. Therefore, the load profile curve cannot track the reference line accurately for those cases, but possesses a reasonable offset. On the other hand, the peak is fully shaved in the 20% case; hence, the reference operating point estimate is more accurate, and the load profile curve tracks the reference line better.

The performance of the proposed algorithm under different

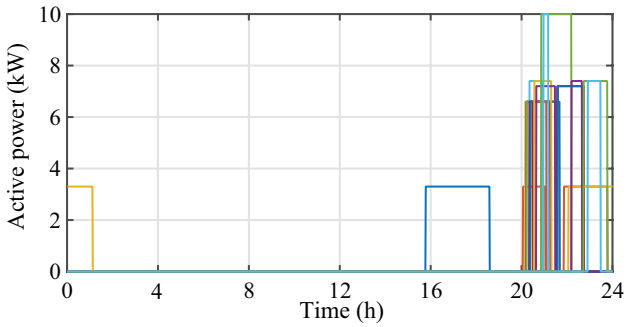

(a)

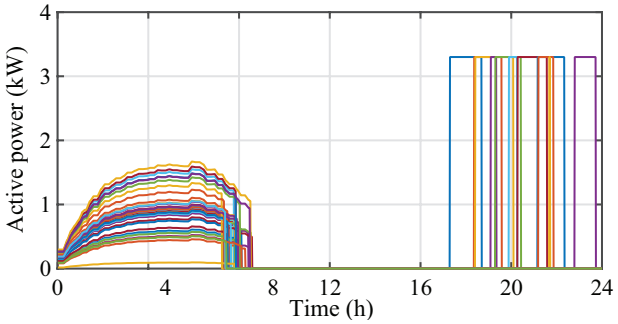

(b)

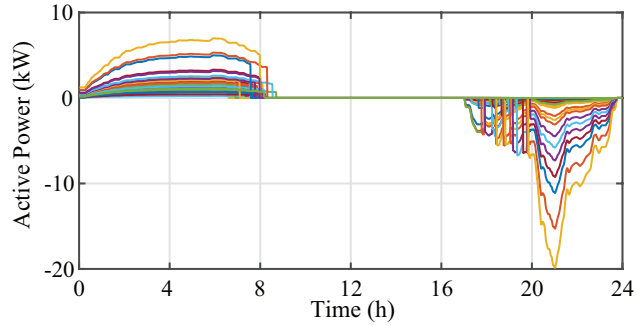

(c)

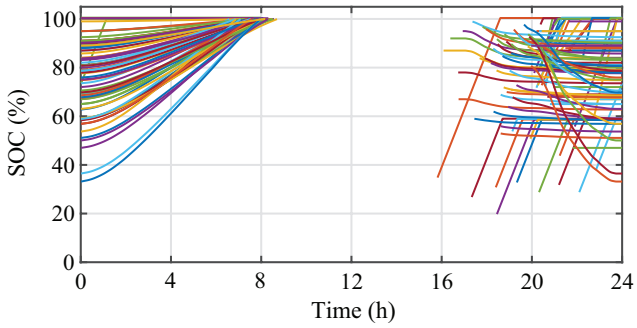

(d)

Fig. 8. Results for individual PEVs for 10% penetration case: (a) uncontrolled charging powers of 20 PEVs, (b) smart charging powers of 40 PEVs, (c) V2G powers of 40 PEVs, and (d) SOC for all PEVs (Each different color stands for charging/V2G power/SOC for a specific vehicle with a total of 100 PEVs).

choices of the reference operating points are evaluated in terms of PSI and MSE. PSI is a measure of the peak shaving performance and calculated as the ratio of the total shaved

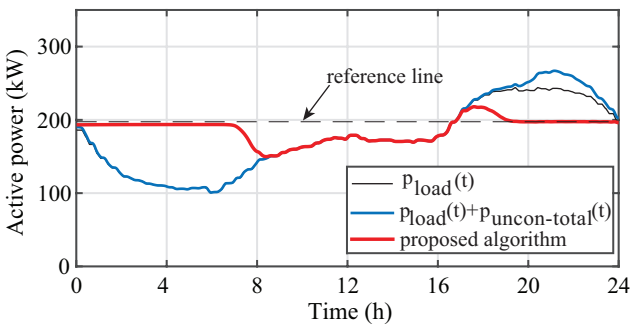

(a)

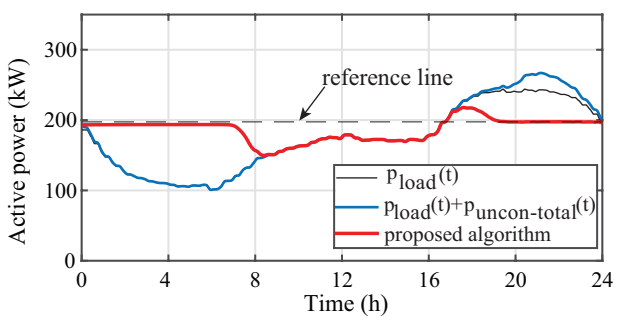

(b)

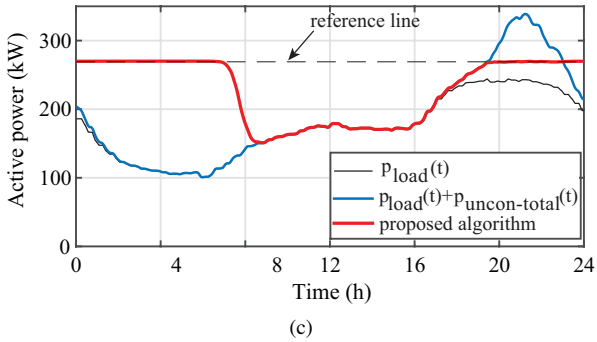

(c)

Fig. 9. Aggregated load profile with proposed algorithm for (a) 5% PEV, (b) 10% PEV, and (c) 20% PEV penetration rates (average of 100 trials).

energy to the peak energy to be shaved as follows:

$$PSI = \frac{\sum_i \int_{t_{peak-start}}^{t_{peak-end}} p_{V2G,i}(\tau) \cdot d\tau}{\int_{t_{peak-start}}^{t_{peak-end}} p_{peak}(\tau) \cdot d\tau} \tag{22}$$

The closer the PSI is to unity, the better the performance. If the reference line is the *desired response, d(n)*, and the resulting load is the *estimator,* $\hat{d}(n)$, in context of estimation theory, MSE can be computed to assess how close the output of the algorithm is to the reference line. MSE is calculated as:

$$MSE = \frac{1}{L} \sum_{n=1}^{L} \left(d(n) - \hat{d}(n)\right)^2 \tag{23}$$

where L is the number of samples in the range of interest, (00:00, $t_{dept-ave}$) ∪ (t_{0-ave}, 24:00). The results of the analysis for different choices of the reference operating point, i.e., DM, MMMP, MPH, and proposed dynamic reference line are presented in Table II. PSI values for the choices of the reference operating point as MPH and dynamic reference point are comparable and significantly greater than that of

TABLE II
COMPARISON OF REFERENCE OPERATING POINT CHOICES USING PROPOSED CHARGING AND DISCHARGING ALGORITHMS

Reference operating point	PEV penetration level					
	5%		10%		20%	
	MSE*	PSI	MSE*	PSI	MSE*	PSI
DM	2508.8	0.80	13761.7	0.88	56470.7	0.94
MMMP	2050.8	0.81	12472.8	0.90	55520.1	0.94
MPH	7898.7	0.96	927.05	0.98	7902.4	1.00
Proposed	34.6	0.90	0.6	0.99	0.3	1.00

*Unit in $(kW)^2$.

other choices for all penetration levels. There is a correlation between the PSI value and the penetration level. As the penetration level increases, PSI of the adaptive algorithm also increases due to increased capacity for the V2G service.

Overall, the proposed control algorithm handles the EVGI impact for different penetration levels successfully and provides a smooth and low-variance load profile by selecting a dynamic reference line to be followed by the PEVs. Selection of the dynamic reference line outperforms the other methods that assume fixed reference line values.

C. Error Analysis

Finally, the algorithm is tested when there are errors in load forecasting, estimation of the number of PEVs and PEV mobility data, and user choice assumptions. We first analyze the impact of the difference between the forecasted and actual load profiles. The mean absolute percentage error (MAPE) is used to measure the quantitatively assessment of forecast performance which is defined as:

$$MAPE = \frac{1}{T}\sum_{t=1}^{T}\left|\frac{p_{load}(t) - \hat{p}_{load}(t)}{p_{load}(t)}\right| \times 100\% \qquad (24)$$

An average of load profile for the last ten weekdays of November 2014 is used as the forecast load for the first weekday of December 2014. The MAPE is calculated as 5.27%. Fig. 10(a) depicts the forecasted and actual non-PEV load profile. The result of the proposed adaptive algorithm for 10% PEV penetration using this base load forecast is shown in Fig. 10(b). The algorithm can shave peak loads without compromising the PEV user convenience, e.g., full SOC at time of departure. However, P_{ref} tracking accuracy is somewhat reduced to an MSE of 443.4 $(kW)^2$, although the variance of the overall consumption remains low. Note that much lower MAPEs (such as 1-2% as reported in [45]) can be achieved, which in turn will improve the performance of the proposed algorithm.

Table III presents the results for 10% PEV penetration when different error sources are considered. The first row of the table refers to the case where all the assumptions are perfect, and the last row refers to the case when all errors are considered jointly. For the case considered in the third row, the number of PEVs are assumed to be 10% less than expected. It is also assumed that each user choice is occurred to be 30%, 35%, and 35% for standard, V1G, and V2G user preferences, respectively, thus deviating from initial expectations. The results regarding this error is shown in Fig. 11. As shown in the figure, the algorithm achieves a satisfactory tracking performance in response to forecasting errors in number of PEVs and user choices. The results in the fourth row are obtained by assuming that the PEVs arrive/leave home according to Gaussian distributions whose means are shifted by 15 min compared to the models built from the historical data. In addition, the mean of the actual daily distance distribution is assumed to be 5 km less than the expected. As may be observed, the peak shaving service, which is invaluable for the utility grid to save the cost of generating expensive energy, is not compromised in any case. Among all the error types, the base load forecasting error returns the highest MSE. The MSE of the other cases are considerably lower. Therefore, it can be concluded that the accuracy of the base load forecast has the greatest impact on the performance of the algorithm. The algorithm can successfully deal with the variations in the number of PEVs, mobility data and user preferences up to a certain extent. Furthermore, all of the PEVs successfully reach full SOC at departure time.

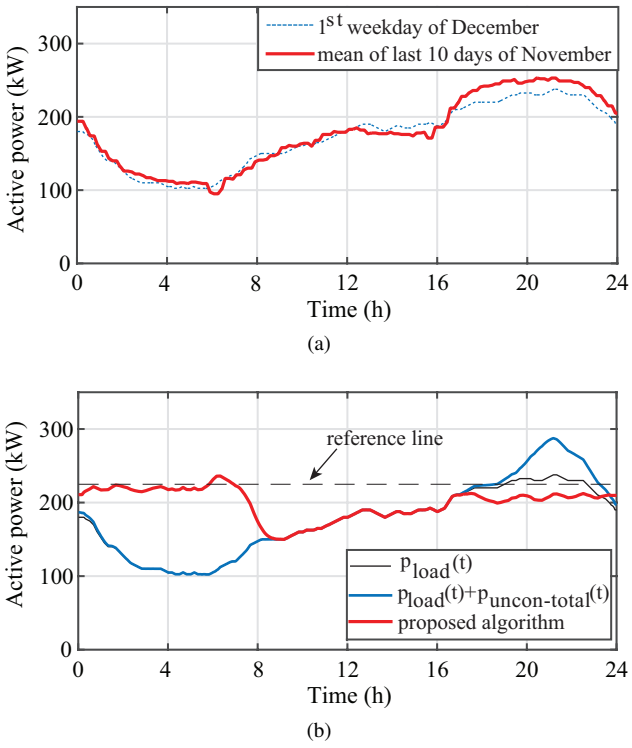

Fig. 10. Behavior of the algorithm in response to load forecasting error: (a) forecasted load and actual load profiles (b) load leveling performance.

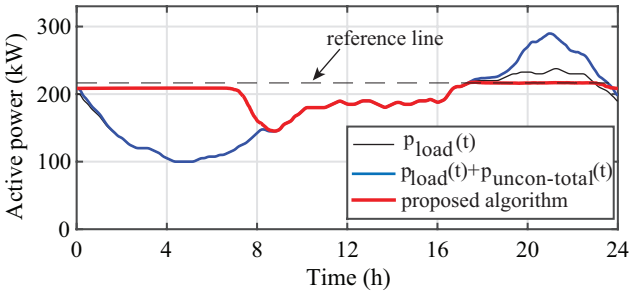

Fig. 11. Aggregated load profile with forecasting errors in number of PEVs and user choices.

TABLE III
PERFORMANCE OF THE ALGORITHM FOR DIFFERENT SOURCES OF ERROR.

Error Type	MSE $(kW)^2$	PSI
No error	1.1	0.98
Base load forecast	443.4	1
Number of PEVs and user choices	124.23	1
Mobility parameters	152.74	0.99
All together	479.5	0.97

Consequently, the reduction of peak-demand is an invaluable service for the utility grid, saving the cost of generating expensive peak energy. In the longer term, peak reduction, as proposed in this study, can be used as a demand response tool that may act as a new cost-efficient distributed generation resource.

V. CONCLUSIONS

This paper introduces an adaptive V2G/discharging and smart charging management scheme for peak shaving and load leveling in a residential distribution grid. A new dynamic reference operating point approach has been proposed to flatten the load profile on a 24-hour basis using the prior knowledge of PEV mobility characteristics and non-PEV base load. Each EV is ensured full SOC at the time of departure. User-convenience and practicability in the field, i.e., reduced computational intensity and bidirectional communication data exchange have also been addressed. The performance of the developed strategy has been tested with heuristic charging policies for various PEV penetration cases. It is shown that it performs better in terms of MSE and PSI values in comparison to fixed reference operating point approaches for all PEV penetration levels considered. For a complete EVGI strategy, future work will include other technical parameters (e.g., voltage drops and feeder losses) in addition to the grid congestion to accommodate more PEVs without any network reinforcement. From the PEV user perspective, the cost of additional battery degradation due to the V2G operation will also be considered.

REFERENCES

[1] T. G. San Román, I. Momber, M. R. Abbad, and Á. S. Miralles, "Regulatory framework and business models for charging plug-in electric vehicles: Infrastructure, agents, and commercial relationships," *Energy Policy*, vol. 39, no. 10, pp. 6360–6375, 2011.

[2] L. P. Fernandez, T. G. San Roman, R. Cossent, C. M. Domingo, and P. Frías, "Assessment of the impact of plug-in electric vehicles on distribution networks," *IEEE Trans. Power Syst.*, vol. 26, no. 1, pp. 206–213, 2011.

[3] E. Veldman and R. A. Verzijlbergh, "Distribution grid impacts of smart electric vehicle charging from different perspectives," *IEEE Trans. Smart Grid*, vol. 6, no. 1, pp. 333–342, 2015.

[4] S. Shafiee, M. Fotuhi-Firuzabad, and M. Rastegar, "Investigating the impacts of plug-in hybrid electric vehicles on power distribution systems," *IEEE Trans. Smart Grid*, vol. 4, no. 3, pp. 1351–1360, Sept. 2013.

[5] W. Kempton and J. Tomić, "Vehicle-to-grid power fundamentals: Calculating capacity and net revenue," *J. of Power Sources*, vol. 144, no. 1, pp. 268–279, 2005.

[6] K. Knezovi, S. Martinenas, P. B. Andersen, A. Zecchino, and M. Marinelli, "Enhancing the role of electric vehicles in the power grid: Field validation of multiple ancillary services," *IEEE Trans. Transport. Electrific*, vol. 3, no. 1, pp. 201–209, Mar. 2017.

[7] M. J. E. Alam, K. M. Muttaqi, and D. Sutanto, "A controllable local peak-shaving strategy for effective utilization of pev battery capacity for distribution network support," *IEEE Trans. Ind. Appl.*, vol. 51, no. 3, pp. 2030–2037, 2015.

[8] J. García-Villalobos, I. Zamora, J. San Martín, F. Asensio, and V. Aperribay, "Plug-in electric vehicles in electric distribution networks: A review of smart charging approaches," *Renewable and Sustainable Energy Reviews*, vol. 38, pp. 717–731, 2014.

[9] M. C. Kisacikoglu, M. Kesler, and L. M. Tolbert, "Single-phase on-board bidirectional PEV charger for V2G reactive power operation," *IEEE Trans. Smart Grid*, vol. 6, no. 2, pp. 767–775, Mar. 2015.

[10] K. M. Tan, V. K. Ramachandaramurthy, and J. Y. Yong, "Integration of electric vehicles in smart grid: A review on vehicle to grid technologies and optimization techniques," *Renewable and Sustainable Energy Reviews*, vol. 53, pp. 720–732, 2016.

[11] M. Singh, P. Kumar, and I. Kar, "A multi charging station for electric vehicles and its utilization for load management and the grid support," *IEEE Trans. Smart Grid*, vol. 4, no. 2, pp. 1026–1037, 2013.

[12] R. Abousleiman and R. Scholer, "Smart charging: System design and implementation for interaction between plug-in electric vehicles and the power grid," *IEEE Trans. Transport. Electrific*, vol. 1, no. 1, pp. 18–25, June 2015.

[13] A. Di Giorgio, F. Liberati, and S. Canale, "Electric vehicles charging control in a smart grid: A model predictive control approach," *Control Engineering Practice*, vol. 22, pp. 147–162, 2014.

[14] S. Deilami, A. S. Masoum, P. S. Moses, and M. A. Masoum, "Real-time coordination of plug-in electric vehicle charging in smart grids to minimize power losses and improve voltage profile," *IEEE Trans. Smart Grid*, vol. 2, no. 3, pp. 456–467, 2011.

[15] K. Kaur, A. Dua, A. Jindal, N. Kumar, M. Singh, and A. Vinel, "A novel resource reservation scheme for mobile phevs in v2g environment using game theoretical approach," *IEEE Trans. Veh. Technol.*, vol. 64, no. 12, pp. 5653–5666, 2015.

[16] N. Leemput, F. Geth, J. Van Roy, A. Delnooz, J. Buscher, and J. Driesen, "Impact of electric vehicle on-board single-phase charging strategies on a flemish residential grid," *IEEE Trans. Smart Grid*, vol. 5, no. 4, pp. 1815–1822, 2014.

[17] K. Valentine, W. G. Temple, and K. M. Zhang, "Intelligent electric vehicle charging: Rethinking the valley-fill," *J. of Power Sources*, vol. 196, no. 24, pp. 10 717–10 726, 2011.

[18] E. Sortomme, M. M. Hindi, S. J. MacPherson, and S. Venkata, "Co-ordinated charging of plug-in hybrid electric vehicles to minimize distribution system losses," *IEEE Trans. Smart Grid*, vol. 2, no. 1, pp. 198–205, 2011.

[19] G. Binetti, A. Davoudi, D. Naso, B. Turchiano, and F. L. Lewis, "Scalable real-time electric vehicles charging with discrete charging rates," *IEEE Trans. Smart Grid*, vol. 6, no. 5, pp. 2211–2220, 2015.

[20] L. Gan, U. Topcu, and S. H. Low, "Optimal decentralized protocol for electric vehicle charging," *IEEE Trans. Power Syst.*, vol. 28, no. 2, pp. 940–951, May 2013.

[21] Z. Wang and S. Wang, "Grid power peak shaving and valley filling using vehicle-to-grid systems," *IEEE Trans. Power Del.*, vol. 28, no. 3, pp. 1822–1829, July 2013.

[22] E. Sortomme and M. A. El-Sharkawi, "Optimal charging strategies for unidirectional vehicle-to-grid," *IEEE Trans. Smart Grid*, vol. 2, no. 1, pp. 131–138, Mar. 2011.

[23] K. M. Tan, V. K. Ramachandaramurthy, J. Y. Yong, S. Padmanaban, L. Mihet-Popa, and F. Blaabjerg, "Minimization of load variance in power grids–investigation on optimal vehicle-to-grid scheduling," *Energies*, vol. 10, no. 11, p. 1880, 2017.

[24] G. Wang, J. Zhao, F. Wen, Y. Xue, and G. Ledwich, "Dispatch strategy of phevs to mitigate selected patterns of seasonally varying outputs from renewable generation," *IEEE Trans. Smart Grid*, vol. 6, no. 2, pp. 627–639, 2015.

[25] L. Jian, H. Xue, G. Xu, X. Zhu, D. Zhao, and Z. Shao, "Regulated charging of plug-in hybrid electric vehicles for minimizing load variance in household smart microgrid," *IEEE Trans. Ind. Appl.*, vol. 60, no. 8, pp. 3218–3226, 2013.

[26] I. Aswantara, K. S. Ko, and D. K. Sung, "A dynamic point of preferred operation (ppo) scheme for charging electric vehicles in a residential area," in *Proc. Connected Veh. and Expo (ICCVE), 2013 Int. Conference on*. IEEE, 2013, pp. 201–206.

[27] N. Erdogan, F. Erden, and M. Kisacikoglu, "A fast and efficient coordinated vehicle-to-grid discharging control scheme for peak shaving in power distribution system," *Journal of Modern Power Systems and Clean Energy*, Jan 2018.

[28] C.-K. Wen, J.-C. Chen, J.-H. Teng, and P. Ting, "Decentralized plug-in electric vehicle charging selection algorithm in power systems," *IEEE Trans. Smart Grid*, vol. 3, no. 4, pp. 1779–1789, 2012.

[29] C. Ahn, C.-T. Li, and H. Peng, "Optimal decentralized charging control algorithm for electrified vehicles connected to smart grid," *J. of Power Sources*, vol. 196, no. 23, pp. 10 369–10 379, 2011.

[30] M. Kisacikoglu, F. Erden, and N. Erdogan, "Distributed control of PEV charging based on energy demand forecast," *IEEE Trans. Ind. Informat.*, vol. 14, no. 1, pp. 332–341, Jan. 2018.

[31] Z. Ma, D. S. Callaway, and I. A. Hiskens, "Decentralized charging control of large populations of plug-in electric vehicles," *IEEE Trans. Control Syst. Technol.*, vol. 21, no. 1, pp. 67–78, 2013.

[32] A. Malhotra, G. Binetti, A. Davoudi, and I. D. Schizas, "Distributed power profile tracking for heterogeneous charging of electric vehicles," *IEEE Trans. Smart Grid*, vol. 8, no. 5, pp. 2090–2099, Sept. 2017.

[33] R. Mehta, D. Srinivasan, A. M. Khambadkone, J. Yang, and A. Trivedi, "Smart charging strategies for optimal integration of plug-in electric vehicles within existing distribution system infrastructure," *IEEE Trans. Smart Grid*, vol. 9, no. 1, pp. 299–312, Jan. 2018.

[34] R. Mehta, D. Srinivasan, A. Trivedi, and J. Yang, "Hybrid planning method based on cost-benefit analysis for smart charging of plug-in electric vehicles in distribution systems," *IEEE Trans. Smart Grid*, vol. PP, no. 99, pp. 1–1, 2017.

[35] Y. He, B. Venkatesh, and L. Guan, "Optimal scheduling for charging and discharging of electric vehicles," *IEEE Trans. Smart Grid*, vol. 3, no. 3, pp. 1095–1105, Sept. 2012.

[36] H. N. T. Nguyen, C. Zhang, and M. A. Mahmud, "Optimal coordination of g2v and v2g to support power grids with high penetration of renewable energy," *IEEE Trans. Transport. Electrific*, vol. 1, no. 2, pp. 188–195, Aug. 2015.

[37] Z. Moghaddam, I. Ahmad, D. Habibi, and Q. V. Phung, "Smart charging strategy for electric vehicle charging stations," *IEEE Trans. Transport. Electrific*, vol. PP, no. 99, pp. 1–1, 2017.

[38] J. Soares, H. Morais, T. Sousa, Z. Vale, and P. Faria, "Day-ahead resource scheduling including demand response for electric vehicles," *IEEE Trans. Smart Grid*, vol. 4, no. 1, pp. 596–605, Mar. 2013.

[39] T. Wu, Q. Yang, Z. Bao, and W. Yan, "Coordinated energy dispatching in microgrid with wind power generation and plug-in electric vehicles," *IEEE Trans. Smart Grid*, vol. 4, no. 3, pp. 1453–1463, 2013.

[40] "Road vehicles-vehicle to grid communication interface," *ISO/IEC Standard 15118*, 2013.

[41] M. Dubaryy and A. Devie, "Battery cycling and calendar aging: year one testing results," Hawaii Natural Energy Institute - University of Hawaii at Manoa, Tech. Rep. HI-12-16, 2016.

[42] (2017, Dec.) Enerjisa Baskent Electric Power Distribution. [Online]. Available: https://www.enerjisa.com.tr/en

[43] F. Erden, M. C. Kisacikoglu, and O. H. Gurec, "Examination of ev-grid integration using real driving and transformer loading data," in *Proc. 2015 9th Int. Conference on Elect. and Electron. Eng. (ELECO)*. IEEE, 2015, pp. 364–368.

[44] EVgo Freedom Station Plans. [Online]. Available: https://www.evgo.com/ev-drivers/freedom-station-plans, [Jan. 28, 2017].

[45] L. Hernandez, C. Baladron, J. M. Aguiar, B. Carro, A. J. Sanchez-Esguevillas, J. Lloret, and J. Massana, "A survey on electric power demand forecasting: future trends in smart grids, microgrids and smart buildings," *IEEE Commun. Surveys Tuts.*, vol. 16, no. 3, pp. 1460–1495, 2014.